Pacific Northwest Climate Sensitivity Simulated by a Regional Climate Model Driven by a GCM. Part I: Control Simulations

L. R. LEUNG AND S. J. GHAN

Pacific Northwest National Laboratory, Richland, Washington

(Manuscript received 8 May 1998, in final form 3 August 1998)

ABSTRACT

A model nesting approach has been used to simulate the regional climate over the Pacific Northwest. The present-day global climatology is first simulated using the NCAR Community Climate Model (CCM3) driven by observed sea surface temperature and sea ice distribution at T42 (2.8°) resolution. This large-scale simulation is used to provide lateral boundary conditions for driving the Pacific Northwest National Laboratory Regional Climate Model (RCM). One notable feature of the RCM is the use of subgrid parameterizations of orographic precipitation and vegetation cover, in which subgrid variations of surface elevation and vegetation are aggregated to a limited number of elevation–vegetation classes. An airflow model and a thermodynamic model are used to parameterize the orographic uplift/descent as air parcels cross over mountain barriers or valleys.

The 7-yr climatologies as simulated by CCM3 and RCM are evaluated and compared in terms of large-scale spatial patterns and regional means. Biases are found in the simulation of large-scale circulations, which also affect the regional model simulation. Therefore, the regional simulation is not very different from the CCM3 simulation in terms of large-scale features. However, the regional model greatly improves the simulation of precipitation, surface temperature, and snow cover at the local scales. This is shown by improvements in the spatial correlation between the observations and simulations. The RCM simulation is further evaluated using station observations of surface temperature and precipitation to compare the simulated and observed relationships between surface temperature–precipitation and altitude. The model is found to correctly capture the surface temperature–precipitation variations as functions of surface topography over different mountain ranges, and under different climate regimes.

1. Introduction

The need for integrated assessment of the impacts of climate change or climate variability on water resources, ecosystems, and agriculture has provided much incentive for climate modelers to consider the use of limited-area models for higher resolution simulations of climate scenarios. To date, there are a number of studies that used a one-way model nesting approach for the simulation of regional climate and climate change (e.g., Giorgi et al. 1994; Hirakuchi and Giorgi 1995; McGregor and Walsh 1994). In the one-way model nesting approach, atmospheric general circulation models (GCM) are used to simulate the large-scale circulation, which then provides the lateral boundary conditions for driving regional climate models (RCM).

Several conclusions on the use of the one-way model nesting approach have been summarized in the 1996 Intergovernmental Panel on Climate Change report (IPCC 1996). First, there is a general agreement from previous studies that regional climate model simulations are affected by errors in the large-scale fields provided by GCMs. Second, the performance of regional climate models improves when the spatial resolution of GCMs increases. However, studies by Risbey and Stone (1996) and Marshall et al. (1997), for example, suggested that increasing spatial resolution may not be the solution to improving the simulation of large-scale circulation, which is a critical input to regional climate models. Both studies concluded that some systematic biases in GCMs cannot be removed simply by increasing spatial resolution. More significant improvements are more likely to result from enhancements in physical parameterizations.

The utility of regional climate models is not to improve the simulation of large-scale circulation. Given the limited size of the model domain, regional climate simulations are constrained by the large-scale conditions provided by the GCMs. Hence regional models should reproduce the large-scale features being fed through the lateral boundaries. In reality, the large-scale features simulated by regional climate models might differ from those simulated by GCMs mainly because of differences in the physical parameterizations used by the models. The latter is sometimes necessary because physical pa-

Corresponding author address: Dr. L. Ruby Leung, Pacific Northwest National Laboratory, P.O. Box 999, Richland, WA 99352.
E-mail: ruby.leung@pnl.gov

© 1999 American Meteorological Society

rameterizations are often scale-dependent, and different climate models tend to be tuned according to the performance of a suite of physical parameterizations chosen to represent different physical processes. Nevertheless, regional simulations should not deviate too much from the GCM simulations, except at the lower atmosphere and on spatial scales influenced by surface boundary conditions.

Therefore, the purpose of using regional climate models is to provide high-resolution simulation of surface variables, which are most affected by topographic, vegetation, or land–sea features that can vary substantially over spatial scales of a few kilometers. Correct modeling over such spatial scales requires not only reasonable treatments of physical processes, but also high spatial resolution to resolve features of the lower boundary conditions. Just how high a resolution is needed to model the climate conditions over complex terrain?

Recently, Leung and Ghan (1995, 1998) introduced a subgrid parameterization of orographic precipitation and surface cover that addresses this issue. Their method bypasses the need for very high-resolution modeling through aggregation of subgrid variations of surface elevation and vegetation into a limited number of elevation–vegetation classes. The parameterization yields separate predictions of precipitation, temperature, snow water equivalent, soil moisture, and surface runoff for a selected number of surface elevation–vegetation classes within each grid cell. For each class, cloud processes are treated using a bulk microphysics parameterization, and land surface processes are modeled using a one-dimensional surface physics scheme. During postprocessing, the simulated fields can be distributed according to high-resolution spatial distributions of surface elevation within each grid cell to yield predictions at the scale of the surface elevation data. Leung and Ghan (1995, 1998) applied this parameterization at 90-km grid resolution in a RCM driven by large-scale analyses over the Pacific Northwest, and found good agreement between simulated and observed surface temperature and precipitation over complex terrain. These simulations produce superior performance and require only one-third of the CPU compared with regional simulations at 30-km resolution but without the subgrid parameterizations. Most regional climate studies used spatial resolution between 40 and 100 km.

The purpose of this paper is to extend the previous work of Leung and Ghan by testing the RCM and the subgrid parameterization under the one-way model nesting formulation. Leung and Ghan (1998) performed a 3-yr simulation with the RCM driven by large-scale analyses for a time period that overlaps the present simulation. By comparing the present RCM and GCM simulations with the RCM simulation reported by Leung and Ghan (1998), we can gain some insights for explaining model biases in the RCM simulation driven by the GCM. These simulations will also serve as control simulations for discussion in an accompanying paper on climate sensitivity to doubling of atmospheric CO_2 concentration. Our geographical focus is on the Pacific Northwest, where complex terrain is a prominent feature. Analyses of the results will focus on evaluation of the larger-scale features simulated by the GCM, comparison of surface climatologies simulated by the GCM and RCM, and detailed evaluation of the RCM for simulating the topographic variations in surface temperature and precipitation. While major improvements in the simulations of large-scale circulation must await important enhancements in the representations of physical processes at the GCM scale, development should proceed with regional climate models to establish their validity for simulating small-scale climate features that are important for climate impact assessment.

2. Numerical experiments

A model nesting approach similar to that of Giorgi et al. (1994) and McGregor and Walsh (1993) is used to simulate the regional climate conditions over the Pacific Northwest. First the National Center for Atmospheric Research (NCAR) Community Climate Model (CCM3) is used to simulate the large-scale atmospheric conditions. The Pacific Northwest National Laboratory Regional Climate Model (PNNL-RCM) is used to downscale the GCM climate simulations. These models will be described in more detail below.

a. Description of CCM3

The NCAR CCM3 is the fourth generation of NCAR's Community Climate Model. It is a global spectral model employing a semi-Lagrangian treatment of moisture transport (Williamson and Rasch 1994). An interactive slab ocean is available as an option to simulate ocean surface temperature. Land surface processes are treated by Bonan's (1996) Land Surface Model. Boundary layer transport is treated by a modified form of the Holtslag and Boville (1993) nonlocal scheme. Deep convection is treated by the parameterizations of Hack (1994) and Zhang and MacFarlane (1995). Stratiform clouds precipitate instantaneously following condensation, with evaporation treated in subsaturated layers below cloud. Cloud radiative properties are parameterized in terms of condensed water, which is parameterized in terms of the column water vapor. Cloud fraction is parameterized in terms of relative humidity, convective mass flux, vertical velocity, and static stability. Shortwave radiative fluxes are calculated at 18 wavelengths using the δ-Eddington approximation (Briegleb 1992). Longwave radiative fluxes are calculated using an absorptivity–emissivity formulation. The treatment of gravity wave drag largely follows McFarlane (1987). A full description of the model is provided by Kiehl et al. (1996), and some circulation statistics are reported by Kiehl et al. (1998a).

Changes in the CCM since CCM2 have resulted in

significant improvements in the simulated climate. For example, changes in the treatment of radiative transfer and cloud optical properties reduced biases in the planetary radiation balance, July surface temperature over the Northern Hemisphere, precipitation over warm land areas, and stationary waves. Changes in the parameterization of boundary layer transport and deep convection reduced the intensity of the hydrologic cycle. Marshall et al. (1997) documented the impact of these changes on the simulated distribution of precipitation. The readers are referred to Kiehl et al. (1998b), Hack et al. (1998), and Hurrell et al. (1998) for discussions on the energy budget, hydrologic cycle, and dynamical aspects of a 15-yr integration with CCM3 driven by observed sea surface temperature (SST).

For the simulation described in this paper, the CCM3 is run at T42 (2.8° lat × 2.8° long) resolution with 18 vertical levels. Monthly mean SST and sea ice thickness are prescribed rather than predicted by the slab ocean model.

b. Description of PNNL-RCM

The PNNL-RCM is based on the hydrostatic version of the Pennsylvania State University–National Center for Atmospheric Research Mesoscale Model 5 (Anthes et al. 1987; Grell et al. 1993). Several physical parameterizations important on climatic timescales have been applied to the model for climate applications. These parameterizations include a two-stream δ-Eddington treatment for shortwave radiation (Taylor and Ghan 1992) and an emissivity approach for longwave radiation (Kiehl et al. 1987), a bulk cloud microphysics scheme that distinguishes liquid and ice phase (Cotton et al. 1986; Ghan and Easter 1992), and a surface physics scheme (BATS) (Dickinson et al. 1993). Grell's parameterization scheme (Grell 1993) is used to treat cumulus convection. For the planetary boundary layer the high-resolution model of Zhang and Anthes (1982) is used. Hence CCM3 and PNNL-RCM use very different parameterizations for most physical processes.

The most noteworthy feature of the RCM is the introduction of a parameterization of subgrid-scale orographic precipitation processes (Leung and Ghan 1995). The parameterization is based on an elevation model that aggregates subgrid variations of surface elevation to a limited number of elevation bands. A simple airflow model and a thermodynamic model are used to account for orographic uplifting of airmass as it crosses over subgrid hills or valleys defined by the elevation bands within each grid cell. Physical processes such as cloud and precipitation, radiation, boundary layer turbulence, and surface physics are all calculated for each elevation band of each grid cell. At the completion of the simulation, variables predicted for each elevation class can be mapped to different geographical locations according to the high-resolution distribution of surface elevation. This mapping yields high-resolution two-dimensional spatial distributions of surface temperature, precipitation, soil moisture, snow water equivalent, and runoff.

To improve the representation of vegetation and hence the simulation of surface processes, Leung and Ghan (1998) further developed a subgrid vegetation scheme based on the surface elevation dependence of vegetation. Taking advantage of the elevation classification already implemented in the climate model, the general framework for the vegetation scheme is such that each elevation band can further be divided into a number of surface cover types. Based on the analysis of high-resolution (1.5 km) topography and vegetation data over the western United States, Leung and Ghan (1998) concluded that about 70% of the subgrid vegetation variability can be accounted for with only one vegetation type (the dominant type) defined for each elevation band of each grid cell. This way, no extra computation is introduced by the subgrid vegetation scheme; the surface physics scheme is simply applied to a different surface cover for each elevation band. Because inland water is an important source of water for the atmosphere, particularly in the arid western United States, larger inland water bodies are specially treated as a separate surface type even if they are not the dominant surface type within an elevation band. Hence, lakes which are normally too small to be represented by climate model grid cells can now be included in the model. A thermodynamic lake model (Hostetler and Bartlein 1990) and the lake ice treatment of Patterson and Hamblin (1988) are used to simulate lake temperature and ice. Leung and Ghan (1998) described a 3-yr simulation where PNNL-RCM was driven by analyzed large-scale conditions. The simulation of surface temperature, precipitation, and lake temperature is comparable to observations.

In the numerical simulation described below, PNNL-RCM was applied to a domain shown in Fig. 1, with horizontal resolution of 90 km and 23 vertical layers. For comparison, the surface elevation representation in CCM3 for the same domain is shown in Fig. 2. Many detailed terrain features such as the Cascades and the Sierra are omitted in the CCM3 topography. The subgrid parameterizations of orographic precipitation and surface cover are applied over the large rectangular region that covers the Pacific Northwest in Fig. 1. On average, 4.5 elevation bands are defined for each model grid cell, and 14 lakes are described by the subgrid land surface cover scheme (Leung and Ghan 1998).

Table 1 shows the percentage area of different elevation classes and Biosphere–Atmosphere Transfer Scheme (BATS) vegetation types defined in the Pacific Northwest when the subgrid elevation model is applied with a single vegetation type (except for lakes) defined for each elevation band. In summary, a majority of areas lies between 0–100 m and 1000–3000 m, with surface vegetation being mostly short grass, evergreen needle leaf tree, and evergreen shrub. By using the subgrid parameterization scheme, surface temperature and pre-

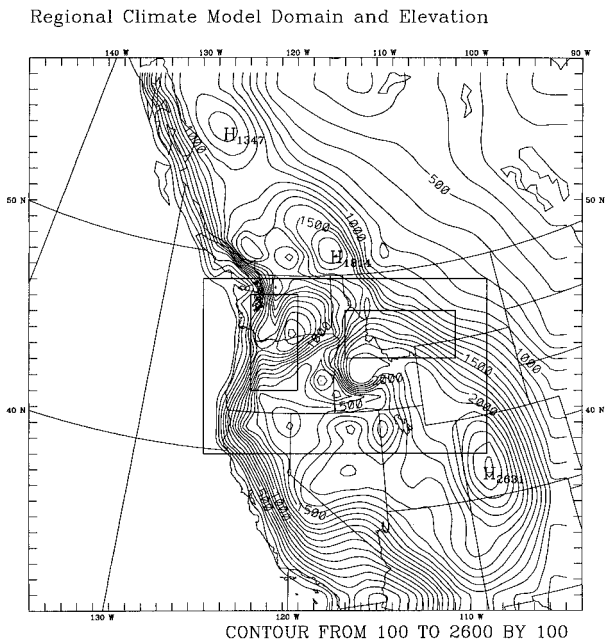

FIG. 1. The domain and surface elevation (m) used by the regional climate model. The subgrid paramterization of orographic precipitation was applied to the rectangular area covering the Pacific Northwest based on aggregation of subgrid surface topography and vegetation at the 1.5-km resolution. Also shown are two smaller rectangular areas over the Cascades and northern Rockies, which are used in the analysis of surface temperature–precipitation and altitude relationships.

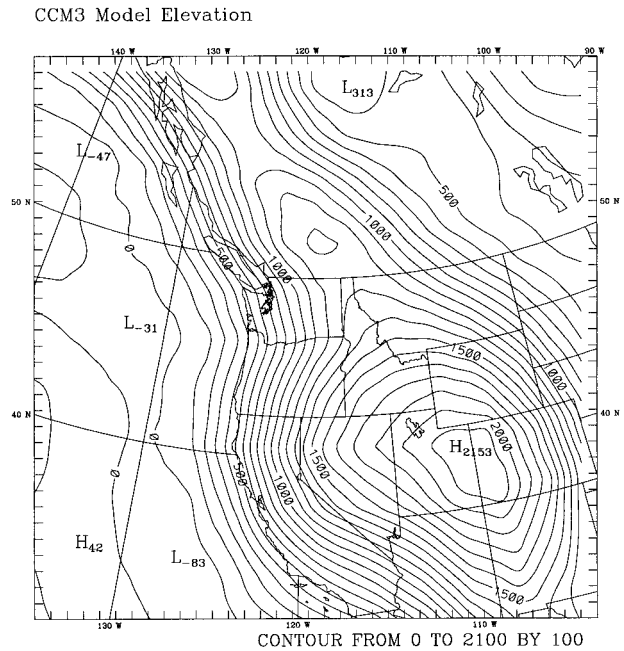

FIG. 2. The surface elevation over the RCM domain used by CCM3.

cipitation, among other climate variables, can be simulated over a wide range of surface elevation in the Pacific Northwest. In section 3c, the simulated relationships between surface temperature and precipitation with altitude will be evaluated using observations from a combination of surface meteorology and SNOTEL stations.

c. Simulation setup

Large-scale and regional-scale simulations have been performed with CCM3 and PNNL-RCM. The CCM3 was driven by observed monthly mean SST and sea ice coverage (Taylor et al. 1997) provided by the Atmospheric Model Intercomparison Project (AMIP II) for September 1988–September 1995 (7 yr). Sea ice thickness is diagnosed from sea ice coverage by assuming the thickness is 2 m if the coverage is 100%, and proportional to the coverage for incomplete sea ice cover.

For the RCM simulation, the CCM3 simulated wind, temperature, water vapor mixing ratio, and surface pressure are interpolated into the lateral boundaries of the RCM and updated every 12 h. A relaxation procedure was used in the RCM to blend the lateral boundary conditions with model predictions within a 10-layer buffer zone on the sides. Following Giorgi et al. (1993), the nudging coefficients decrease exponentially from the outermost layer toward the interior domain.

In the GCM simulation, CCM3 was initialized using the nominal 1 September initial conditions from NCAR and allowed to run for 1 month before the simulations are used to drive PNNL-RCM. The RCM simulations were initialized using atmospheric conditions generated by the CCM3 experiments. Initialization of soil moisture follows that of Giorgi and Bates (1989), and the whole domain is assumed snow free when the simulation begins on 1 October.

3. Model climatologies

This section focuses on evaluation of the large-scale and regional-scale climatologies simulated by CCM3 and PNNL-RCM. Besides comparing the simulated climatologies with observations, we will contrast the climatology simulated at the GCM scale with that at the RCM scale. Simulation results and observations will be shown only within the RCM domain (Fig. 1). Observed large-scale circulations are derived from the National Center for Environmental Prediction (NCEP)–NCAR (NCEP–NCAR) reanalysis for the same period as the simulation. Observed surface temperature and precipitation are obtained from two datasets at different resolutions: the 2.5° resolution surface climatology prepared by Shea et al. (1990) and the 0.5° resolution surface climatology prepared by Legates and Wilmott (1990a,b). These data are used to compare with the CCM3 and RCM results, respectively. We also use surface temperature and precipitation data directly archived from surface meteorology and SNOTEL stations for detailed analyses discussed in sections 3b and 3c.

TABLE 1. Percentage coverage of elevation and land cover classes in the Pacific Northwest. Land cover is defined according to the BATS classification: 1—crop, 2—short grass, 3—evergreen needle leaf tree, 8—desert, 9—tundra, 10—irrigated crop, 14—inland water, 15—ocean, 16—evergreen shrub, 17—deciduous shrub, 18—mixed tree.

Elevation (m)	1	2	3	8	9	10	14	15	16	17	18	% Area
0–100	0.24	—	0.19	—	—	0.13	0.01	17.50	—	—	0.41	18.49
100–200	0.15	—	0.78	—	—	—	—	—	0.11	0.17	0.48	1.69
200–300	0.30	0.02	0.48	—	—	—	—	—	0.11	0.11	0.37	1.39
300–400	0.46	0.05	0.49	—	—	—	—	—	0.14	0.10	0.25	1.49
400–500	0.26	0.07	0.35	—	—	—	—	—	0.33	0.03	0.34	1.39
500–700	0.26	0.21	0.90	—	—	—	—	—	0.98	0.02	0.75	3.11
700–1000	0.04	4.80	1.97	—	—	—	—	—	1.54	—	1.06	9.40
1000–1500	0.18	6.52	5.34	1.16	—	—	0.54	—	8.13	—	1.33	23.20
1500–2000	—	4.54	7.07	—	—	—	—	—	10.58	—	0.13	22.33
2000–3000	—	5.47	4.99	—	0.01	—	—	—	3.36	—	2.70	16.53
3000–4000	—	0.02	0.62	—	0.07	—	—	—	—	—	0.28	0.98
% Area	1.89	21.69	23.17	1.16	0.09	0.13	0.55	17.5	25.28	0.43	8.11	100.0

a. Spatial distribution

To compare the general spatial features simulated by CCM3 and RCM, the CCM3 simulation is interpolated to the RCM model grid cells. For the RCM simulations, the results shown here are aggregated from the subgrid elevation–vegetation classes to the 90-km grid cells to show only the mesoscale features.

1) LARGE-SCALE CIRCULATION

During winter (December–February), the CCM3 simulation of the 500-mb geopotential height (not shown) is generally higher than the observations over the ocean, but lower over land, suggesting a warm bias over the ocean and cold bias over land in the atmospheric column. During summer (June–August), there is a general positive bias everywhere, except over Canada and the surrounding ocean. Hence the summer atmospheric temperature is mostly too warm in the CCM3 simulation. The RCM simulated 500-mb geopotential height (not shown) is very similar to the CCM3 simulation; the difference between the two model simulations is generally less than 8 m, with the RCM simulation being lower.

Moisture transport exerts major control over precipitation in the western United States. Figure 3 shows the bias in the model-simulated 850-mb moisture transport when compared with observations. During winter, CCM3 transports more moisture from northwesterly flow to the Pacific Northwest region and Canada than the observations. This is consistent with the bias in the 500-mb geopotential height, which induces cyclonic circulation that enhances the northwesterly flow near the northern Pacific coast. During summer, biases are mainly confined to the U.S. west coast; about twice as much moisture is being transported by northerly flow in CCM3 along the coastal areas when compared with observations. Again, this reflects the bias in the 500-mb geopotential height. The high pressure center over the Pacific Ocean directs northwesterly flow toward the Pacific Northwest coast, which then turns northerly along the west coast.

Figure 4 compares the CCM3 and RCM simulation of moisture transport at 850 mb during winter. The RCM simulation of moisture transport resembles that of the CCM3 in terms of large-scale features. However, differences show up at the mesoscale where the RCM moisture transport is clearly influenced by surface topography. For example, a sharper gradient is found in the moisture transport across the Cascades, hence producing higher moisture convergence over the mountain, and less moisture is transported inland over the Rockies. Similar areas with stronger moisture convergence are also found on the western side of the Rockies. These features can be simulated only with a higher resolution representation of surface topography.

2) PRECIPITATION

As a result of biases in the CCM3 simulated moisture transport, biases are found in the simulated precipitation as well. Figure 5 shows the bias in the CCM3 simulation when compared with the 2.5° climatology. During winter, because more moisture is being transported to the Pacific Northwest area in the CCM3 simulation, a positive bias is found in the precipitation over the Pacific Northwest, and negative bias of similar magnitude is found over the adjacent ocean. During summer, the bias in precipitation reflects the bias in the southerly flow and moisture convergence over the west coast in the CCM3 simulation. Hence, a negative bias in precipitation is found in the northern coast near Canada, and a positive bias is found over the California coast. Positive bias is also found over the Rockies as a result of the bias in westerly flow simulated by CCM3, which brings more moisture to the Rockies.

Figure 6 compares the CCM3 and RCM simulations with the higher resolution 0.5° precipitation climatology. Using the higher resolution topography representation, RCM correctly puts more precipitation along the

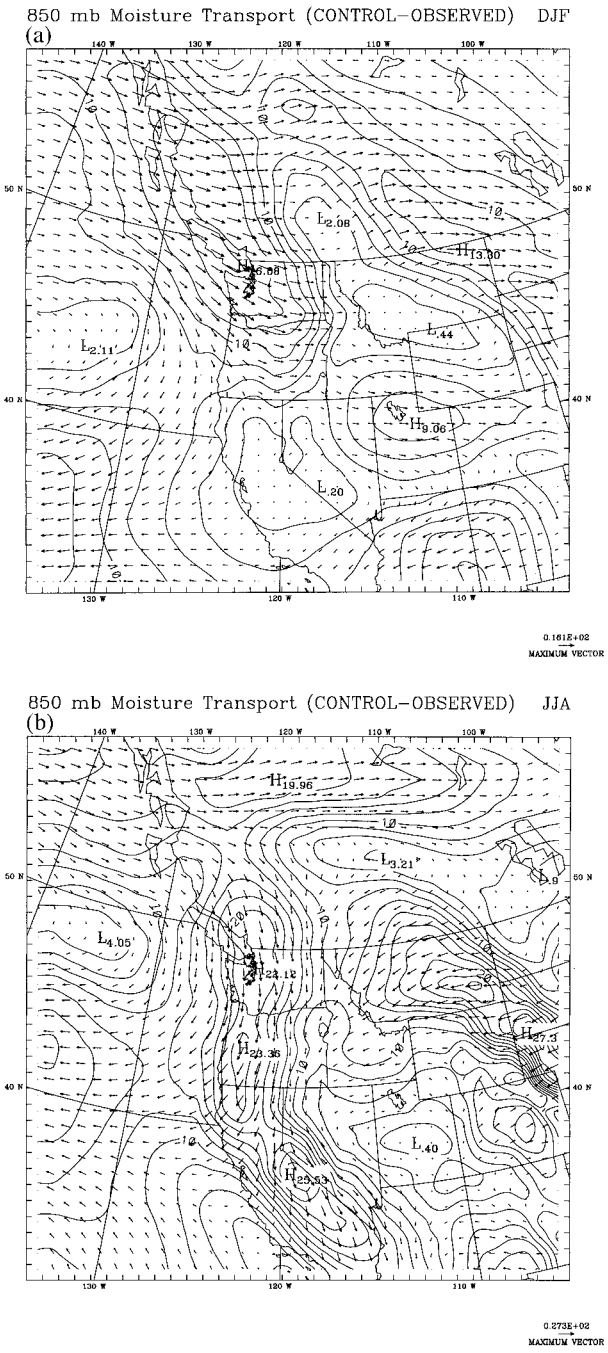

FIG. 3. The difference between the control CCM3 simulated and NCEP–NCAR reanalyzed 850-mb moisture transport shown in vectors for the transport and in contours (2 g kg^{-1} m s^{-1} intervals) for the magnitude.

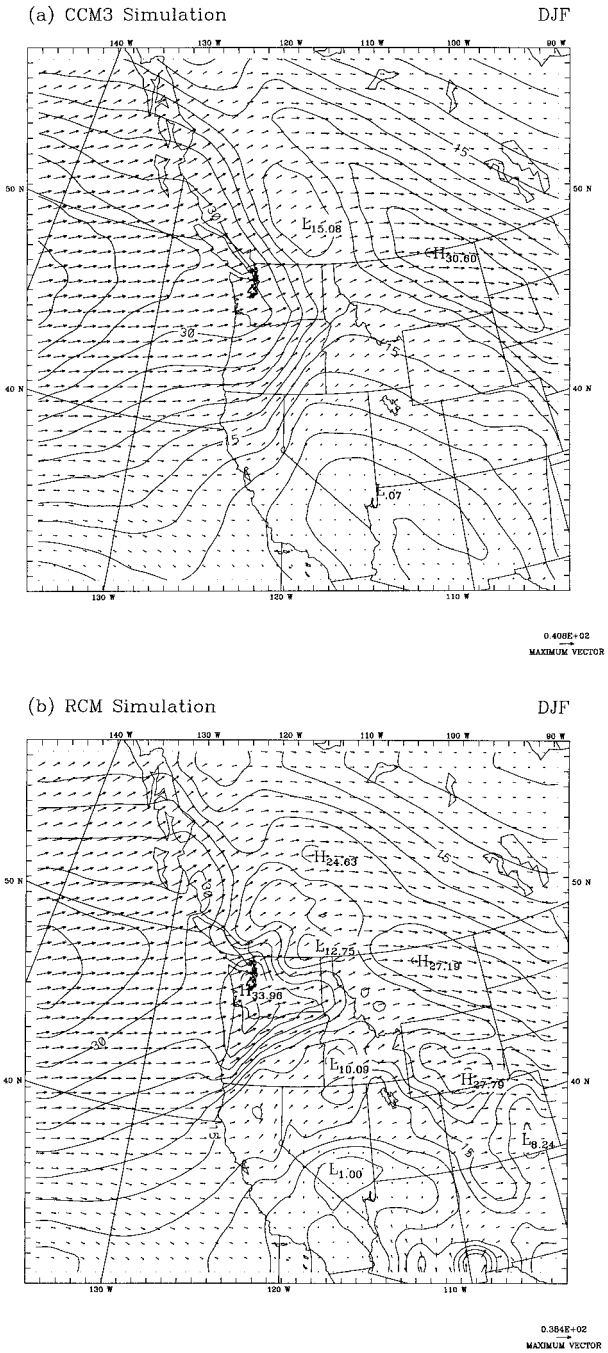

FIG. 4. The CCM3- and RCM-simulated 850-mb moisture transport for Dec–Feb (DJF). Contours are in 3 g kg^{-1} m s^{-1} for the magnitude and the transport is shown in vectors.

coastal areas, hence allowing less moisture to proceed inland to form precipitation. However, the precipitation on the lee side of the Cascades is still too high. The use of higher explicit resolution in RCM might help alleviate this problem. The bias in the large-scale moisture transport simulated by CCM3 has effects on the RCM simulation; RCM also simulated more precipitation along the coast and less precipitation over the adjacent ocean, as in the CCM3 simulation during winter. During summer (not shown), the bias in the RCM simulation again resembles that in the CCM3, except over the Rockies where positive bias in CCM3 is replaced by more widespread negative biases in RCM. The representation of surface topography and the difference in

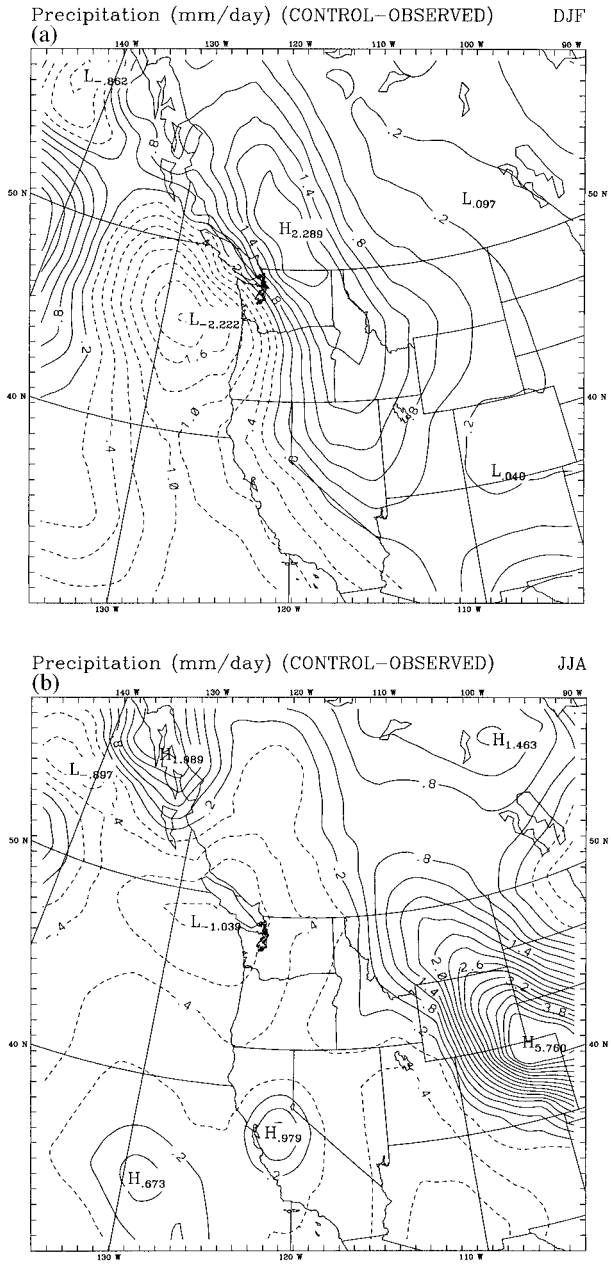

FIG. 5. The difference between the CCM3 and observed precipitation (mm day^{-1}) for DJF and Jun–Aug (JJA). Observations are based on Shea et al. (1990) climatology at 2.5° resolution. Contours are in 0.3 mm day^{-1}.

convective and surface physics parameterizations used are likely to be responsible for such differences between the summer CCM3 and RCM simulated precipitation.

3) SURFACE TEMPERATURE

Figure 7 shows the biases in the CCM3 simulated surface temperature when compared with the 2.5° climatology. The simulation is mostly too cold during winter except near the northeast corner, which happens to run along the east side of the Rockies according to the CCM3 topography (Fig. 2), where the CCM3 topography is generally lower than the actual topography as shown, for example, in Fig. 1. Hence bias in the CCM3 topographic representation can partially explain the pattern of the bias in surface temperature. During summer, warm biases are found near the southern coastal areas, and cold biases are found mostly inland over the Rockies.

Figure 8 compares the spatial distribution of observed surface temperature at 0.5° resolution and that simulated by the models. The RCM simulation clearly captures more of the spatial variability associated with land–sea contrast and surface topography. Hence biases are lower in the RCM than the CCM3 simulation. The RCM bias over the ocean is also lower than that of the CCM3. Since both models use the same SST as lower boundary conditions, this difference is due to vertical transport, which is treated differently in the models.

b. *Regional analysis*

Regional averages and seasonal cycles are the focus of the analyses presented in this section. To evaluate the model-simulated regional means, surface meteorology and SNOTEL station observations over Washington (WA), Oregon (OR), Idaho (ID), and Montana (MT) are simply averaged to form monthly regional means. The CCM3 simulation is interpolated bilinearly from the CCM3 grid cells to the station locations to form regional means. The RCM simulation is interpolated based on linear interpolation with elevation from the RCM elevation–vegetation classes to the station elevation, and bilinear interpolation from the four RCM grid cells closest to the station, and then averaged to form regional means. The observed mean seasonal cycles are calculated based only on the 1988–95 station data.

1) PRECIPITATION

Figure 9 shows the seasonal cycles in precipitation as simulated by CCM3 and RCM and compared with observations. Both models simulated the strong winter peak in precipitation over WA and OR, and the summer peak over MT very well, although biases are also apparent. Obviously, both the winter maximum and summer minimum in precipitation over WA and OR are exaggerated by the models. As already discussed above, these biases are mostly results of biases in the simulation of large-scale circulation. This conclusion is also supported by a previous simulation performed by Leung and Ghan (1998) in which RCM was driven by large-scale analyses for the period 1991–94: the biases in the 3-yr averaged monthly simulated precipitation are less than 0.5 mm day^{-1} over WA and OR, and 0.2 mm day^{-1}

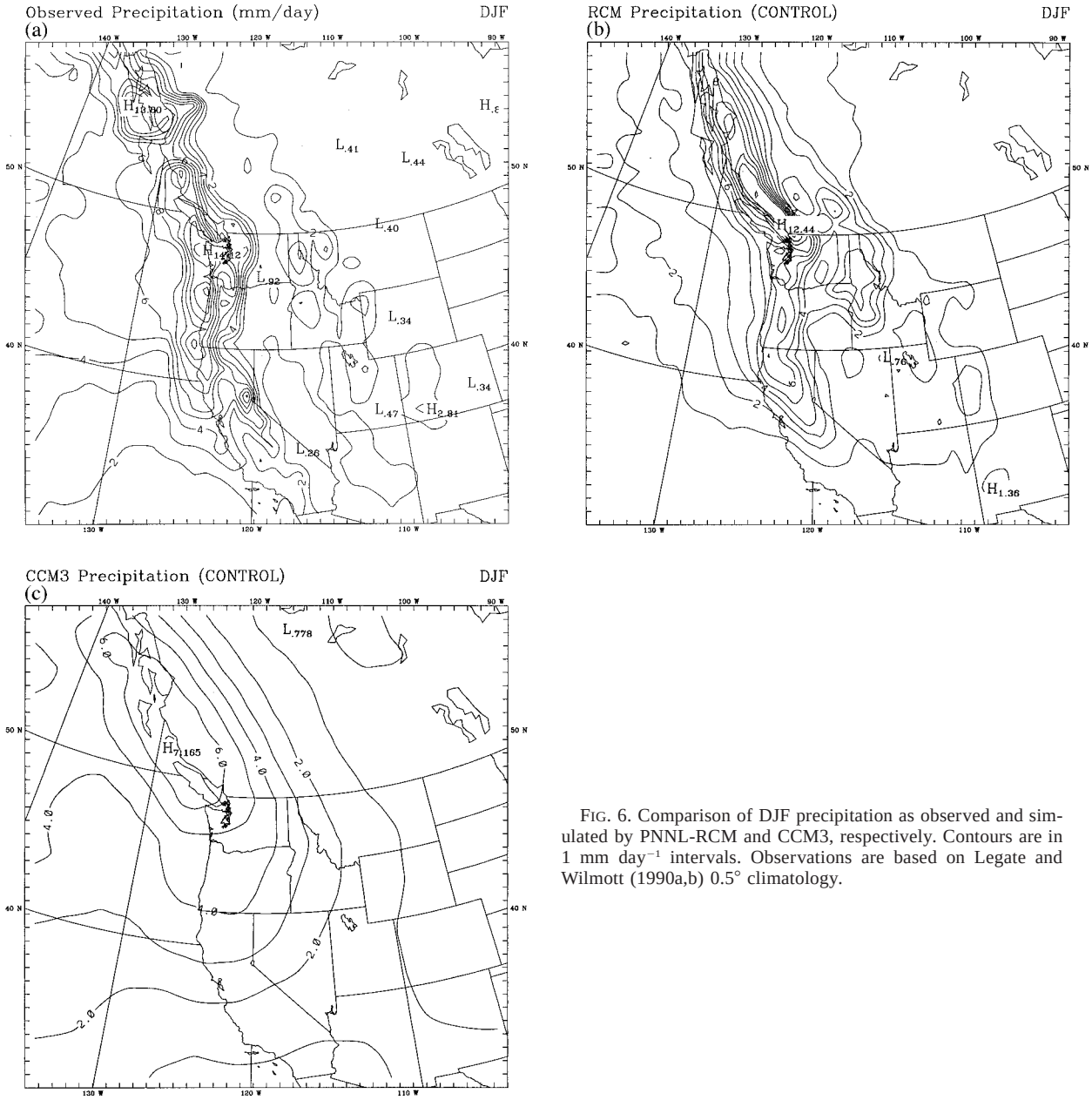

FIG. 6. Comparison of DJF precipitation as observed and simulated by PNNL-RCM and CCM3, respectively. Contours are in 1 mm day^{-1} intervals. Observations are based on Legate and Wilmott (1990a,b) 0.5° climatology.

over ID and MT, compare to 2 and 1.5 mm day^{-1}, respectively, in this simulation where RCM was driven by CCM3.

Two characteristics in Fig. 9 are to be noted here. First, there is little difference between the CCM3- and RCM-simulated regional mean during wintertime when precipitation is mostly associated with the passing of synoptic systems. The difference between the models is larger during spring and summer when precipitation is more convective in nature, and different convective and surface physics parameterizations are used by the models. Second, larger differences between the CCM3- and RCM-simulated regional means are found over ID and MT. In MT, the RCM simulation is lower than the CCM3 simulation during all seasons, and is much closer to the observations.

Similar to the mean precipitation, the simulated interannual variability (not shown) is mostly larger than the observed during winter and less during summer. The difference between the CCM3 and RCM variability follows closely the difference in the mean precipitation simulation. The bias in the RCM model-simulated precipitation is mostly within the natural variability of precipitation. The same is true for the CCM3 simulation, except over MT, where the CCM3 positive bias is above the natural variability.

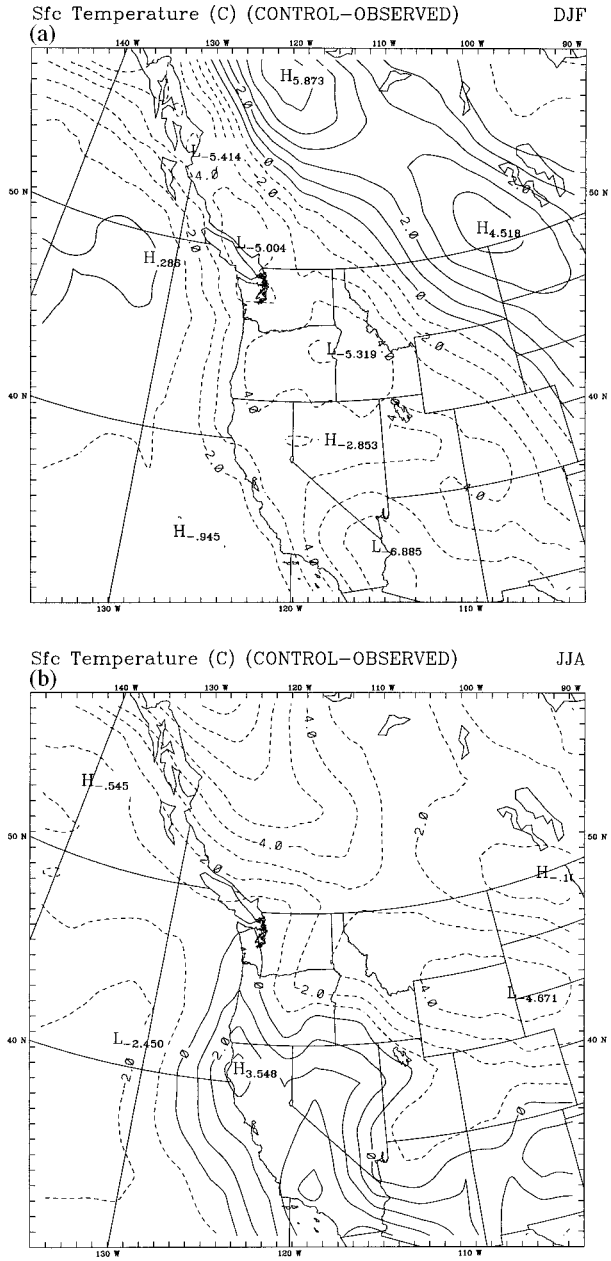

FIG. 7. Similar to Fig. 5 but for surface temperature. Contours are in 1°C interval.

2) SURFACE TEMPERATURE

Figure 10 shows the simulated and observed surface temperature over the four regions. The RCM simulated the surface temperature during winter rather well. Larger biases are mostly found during spring with magnitude up to 5°C, and the simulation tends to be too warm in the summer, which is consistent with the dry bias in the precipitation simulation. Hence the seasonal cycle in surface temperature is exaggerated, especially over MT.

The CCM3-simulated surface temperature is generally lower than the RCM simulation. Over WA, the difference between the simulations is nearly constant throughout the season. Noting that the CCM3 mean topography over WA is about 250 m higher than that of RCM, the difference of about 2°C is at least consistent with the topographic bias in CCM3. Over OR and ID, the difference between the two simulations is rather small and again, shows no variations with seasons. The CCM3 mean topography over those regions is less than 100 m higher than the RCM. Over MT, difference between the models is only found during summer and fall, with RCM up to 5°C warmer than CCM3. Since the difference between the RCM and CCM3 precipitation in MT is not particularly season dependent, difference in cloudiness cannot be responsible for the difference in simulated surface temperature. The difference is more likely to be a result of differences in vegetation and soil representation, and the land surface parameterization schemes. This is again supported by the simulation performed by Leung and Ghan (1998) where RCM was driven by large-scale analyses over 1991–94: warm bias of up to 4°C was also found over ID and MT. This suggests some possible roles of the RCM land surface representation or parameterization in generating the bias.

3) SURFACE SENSIBLE AND LATENT HEAT FLUXES

To partially explain the differences between the RCM and CCM3 simulations of surface temperature and precipitation, we plotted in Fig. 11 the seasonal cycles of monthly averaged surface sensible (SH) and latent (LH) heat fluxes simulated by the models. First it is noted that the sum of SH and LH simulated by the models are within 10 W m^{-2}, suggesting that the total of other surface energy fluxes (net solar heat flux, upward longwave flux, and heat flux to subsurface) are also similar. When SH and LH are studied individually, over WA and OR both models show strong seasonal cycles in the sensible heat flux with maximum over July, and weaker seasonal cycles in the latent heat flux with maximum over May. Furthermore, the differences between the RCM and CCM3 simulations are relatively small except during summer when the RCM sensible heat flux is lower, and the latent heat flux is higher than that of CCM3. Hence the Bowen ratio simulated by RCM is somewhat smaller. Over WA and OR, RCM defines a mixture of vegetation types including evergreen needle leaf trees, evergreen shrubs, and irrigated crops. Only evergreen needle leaf trees are defined in CCM3 over those regions. This may explain some differences in the simulated Bowen ratio.

Over MT, the seasonal maximum heat fluxes are shifted by about 1 month later than those over WA and OR. Differences between the RCM and CCM3 simulations are more pronounced during summer and in ways opposite to those over WA and OR—the RCM sensible heat flux is higher, and the latent heat flux is lower, both

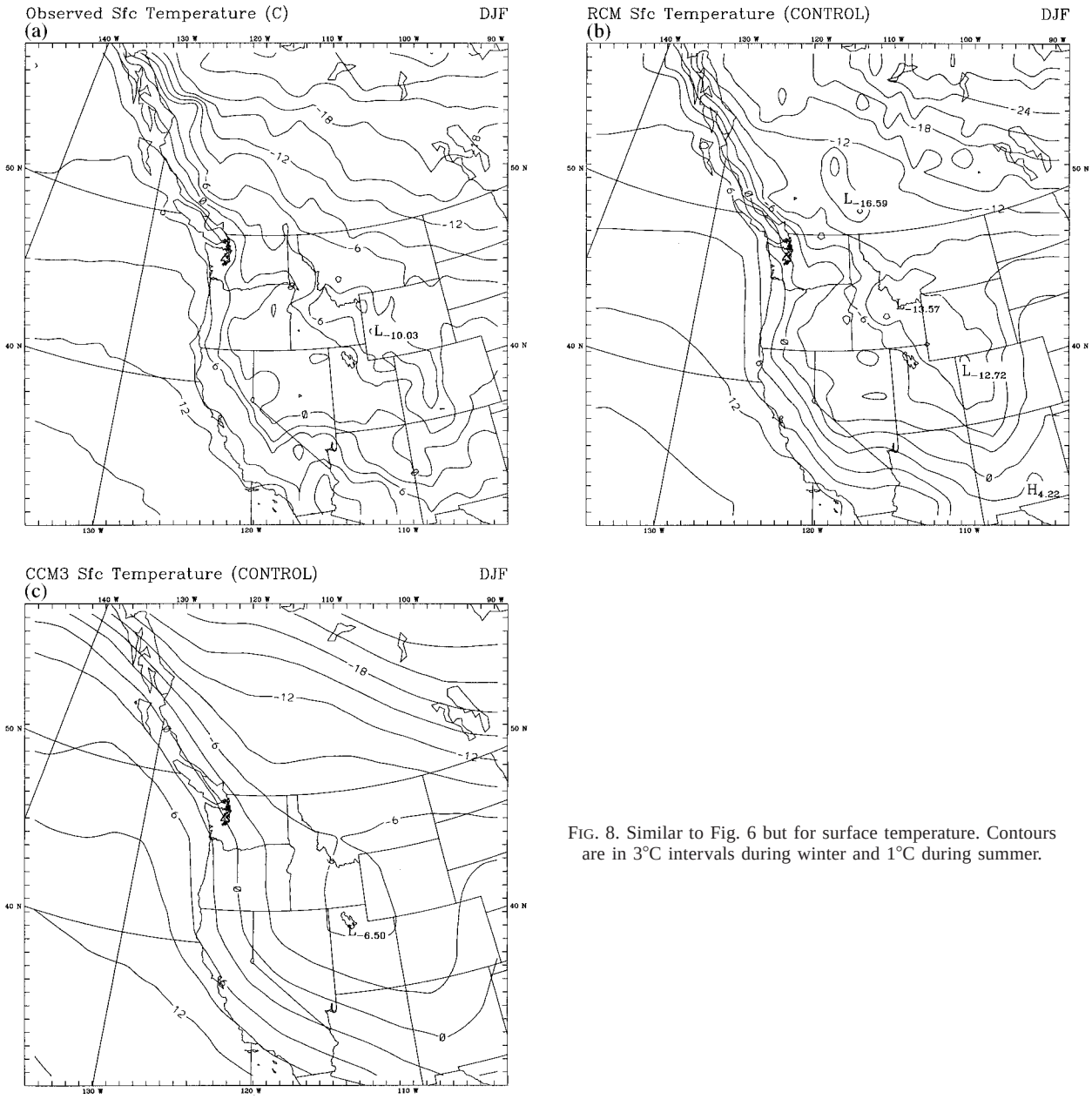

FIG. 8. Similar to Fig. 6 but for surface temperature. Contours are in 3°C intervals during winter and 1°C during summer.

by about 50 W m^{-2} than the CCM3 simulation. This is consistent with the warmer and dryer conditions simulated by RCM as reflected in the surface temperature and precipitation simulation. Again differences in vegetation cover defined by the models may contribute to differences in the surface fluxes and temperature simulations. RCM defines a mixture of evergreen needle leaf trees and short grass over MT; CCM3 defined only evergreen needle leaf trees.

It should also be noted that the surface fluxes simulated by the models over MT are comparable during the cold season. Since the surface temperature and surface sensible and latent heat fluxes simulated by both models are also similar, the reduced precipitation as simulated by RCM compared to CCM3 during winter is not related to differences in moisture transport from the surface, but rather related to reduced atmospheric moisture in the RCM, which could result from blocking effects of the coastal mountains as shown in Fig. 6.

The conditions over ID are intermediate between those of WA–OR and MT. Differences between model simulated fluxes are generally small, except during late spring and early summer (April–June) where the RCM simulated Bowen ratio is much higher than that of CCM3. This is reflected in the much higher precipitation simulated by CCM3 during that period. One possible

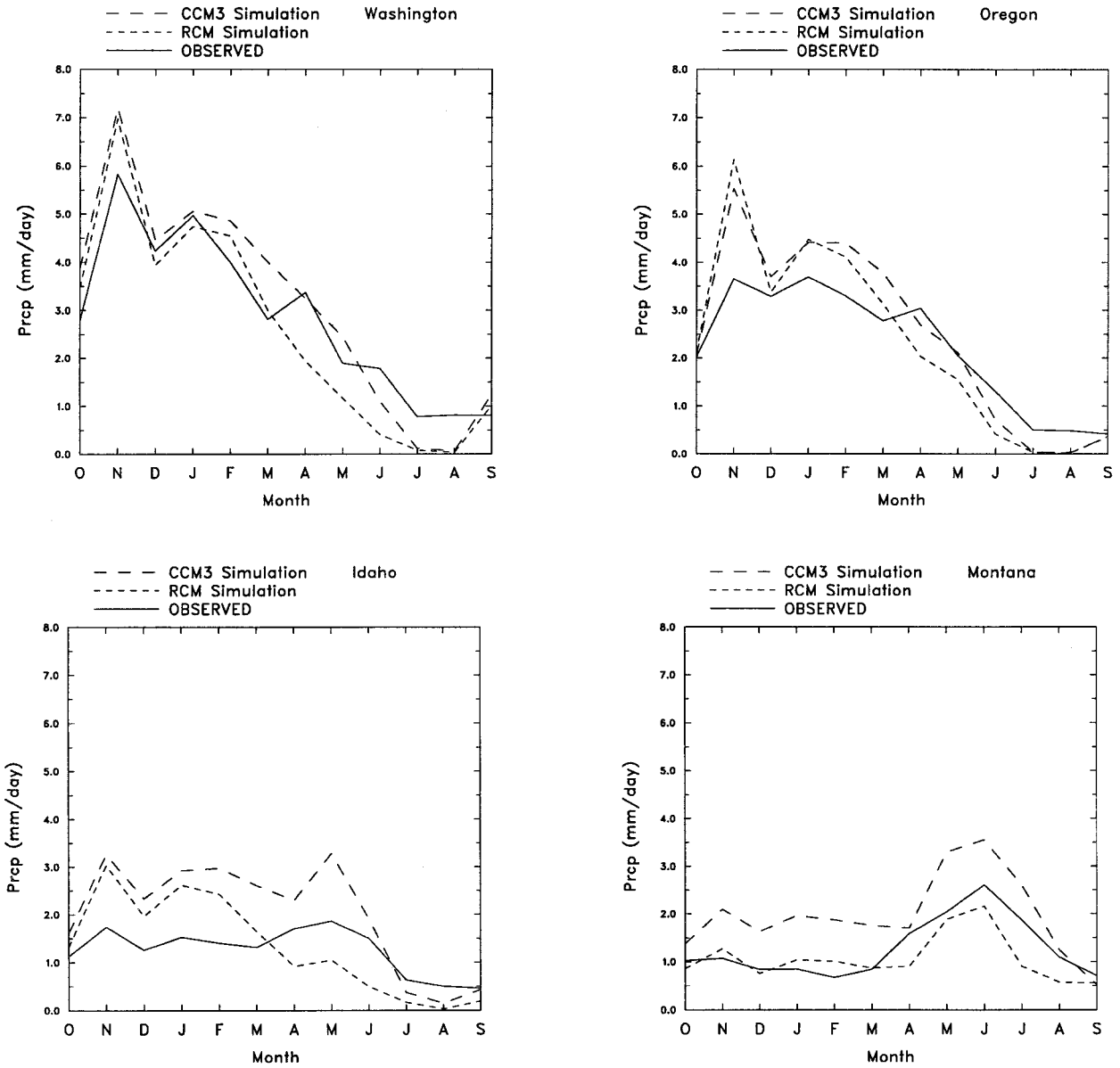

FIG. 9. Comparison of the observed (solid) and CCM3 (long dash) and PNNL-RCM (short dash) simulations of the monthly regional mean precipitation over four regions in the Pacific Northwest.

reason for the differences is the different convective parameterizations used by the models. During the transition period, convection might have been activated more in CCM3 than RCM.

4) SNOW COVER

Over the Pacific Northwest, snow cover can vary strongly at spatial scales of a few kilometers as precipitation and surface temperature follow the complex terrain. The ability to simulate the regional mean precipitation and surface temperature does not translate to the ability to simulate snow cover because it is only over areas at high elevation where temperature is below freezing that precipitation takes the form of snow. The use of smoothed topography such as is in GCMs greatly reduces the possibility for snow formation in mountainous areas.

To compare the CCM3 and RCM simulated snow water equivalent (SWE), Fig. 12 compares the regional mean simulation with observation averaged over the SNOTEL stations in each state. There are about 30 stations over WA and 70 stations over each of the other states. Again, model simulations are interpolated to the station locations using the same method as adopted for precipitation and surface temperature. As most SNO-

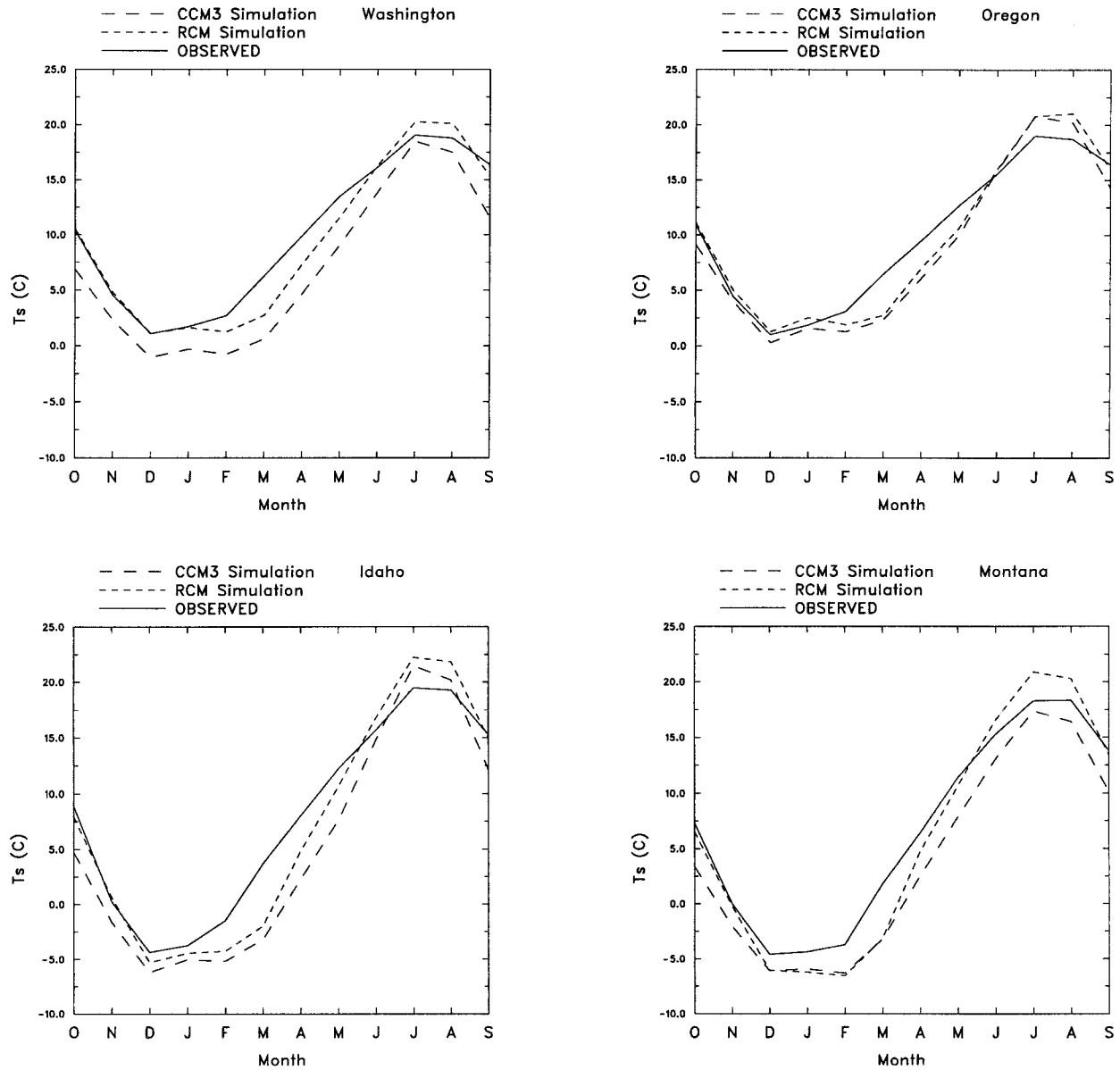

FIG. 10. Similar to Fig. 9 but for monthly regional mean surface temperature.

TEL stations are located at higher elevations (above 1000 m), the regional means are not truly regional averages. Hence this comparison highlights model differences at high elevations.

Clearly, because of the smoothed topography adopted by CCM3, the SWE simulated by CCM3 is too small compared to the observation. The RCM simulation agrees much better with observations than the CCM3 simulation. Generally, the RCM simulated SWE is higher than the observed, which is consistent with the wet and cold bias during winter as shown in Figs. 9 and 10. Furthermore, despite the warm bias in the RCM simulation during summer, the strong cold bias during spring inhibits snowmelt such that the SWE remains higher than observed throughout the seasons, except in MT. Besides the wet and cold bias, the treatment of snow in the surface physics scheme may also be responsible for the snow melting too slowly; however, more evaluation is needed to determine if, and which components of, the BATS surface scheme could be enhanced for improved simulation of SWE.

5) IMPACTS OF DOWNSCALING WITH THE SUBGRID PARAMETERIZATION

From the discussion above, two main factors are found to be responsible for the differences seen in the CCM3 and RCM simulations. First, the two models use

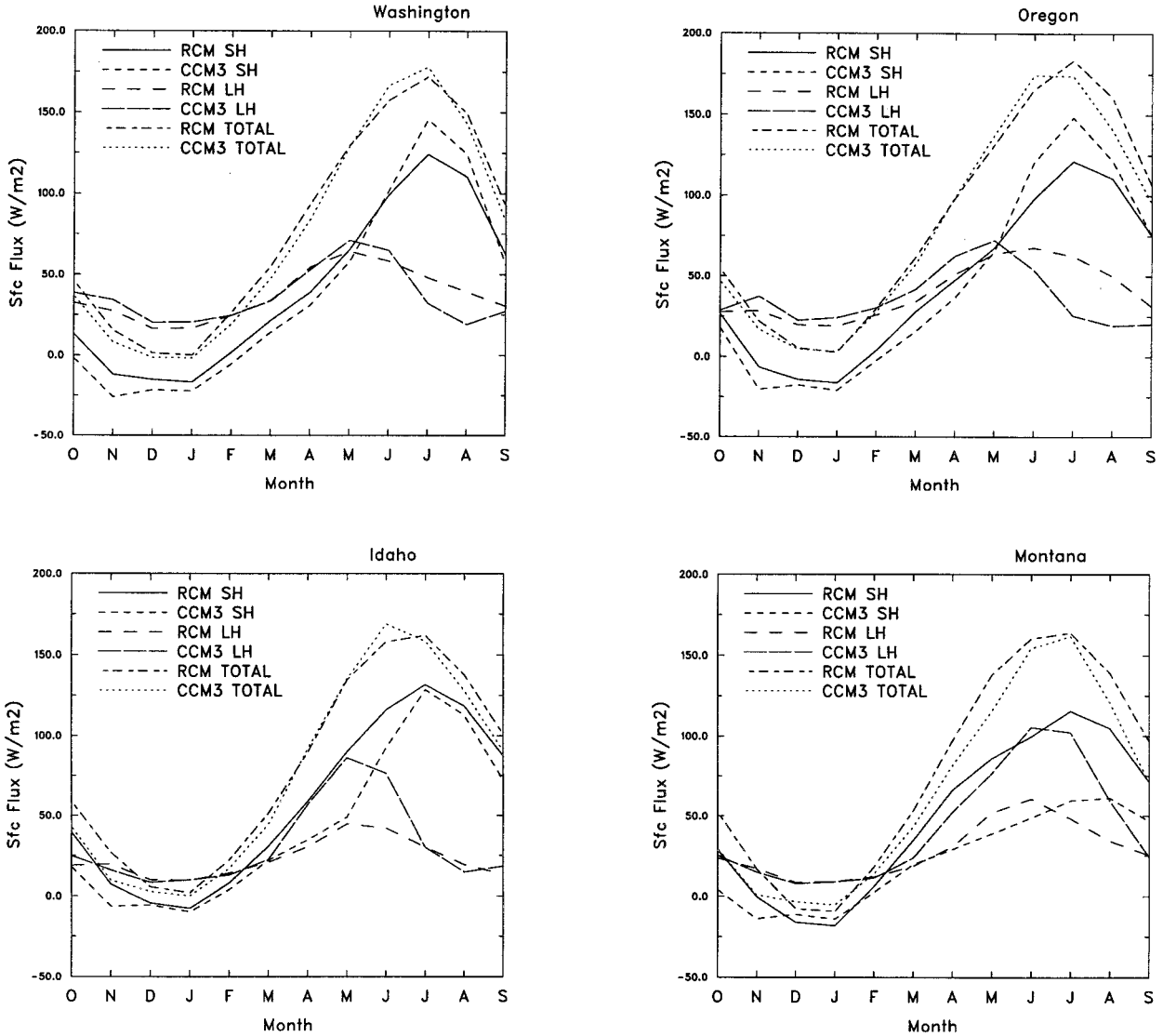

FIG. 11. Similar to Fig. 9 but for SH, LH, and their sum (TOTAL) as simulated by PNNL-RCM and CCM3.

rather different physical parameterizations of cloud, precipitation, and land surface processes. Second, RCM uses a downscaling technique to represent subgrid variability due to topography and land surface cover. To what extent are differences between the CCM3 and RCM simulations due to these factors?

To help answer this question, we have performed a 1-yr simulation (called RCM-ns) with RCM driven by CCM3, but without the use of the subgrid parameterization of orographic precipitation and land surface cover. This 1-yr simulation is compared with the CCM3 simulation and the RCM simulation with the subgrid parameterization, called RCM-s, for the same year. For simplicity, only results from WA will be shown.

Figure 13a shows the model-simulated precipitation. The RCM-ns simulation is always higher than the CCM3 simulation during the cold season, but lower during the warm season. The difference between their monthly means can be as high as 40% during winter and 80% during spring and early summer. This difference can arise from the higher spatial resolution used in the RCM (90 km), which allows the development of mesoscale features or differences in the physical parameterizations used. Comparing the RCM-ns and RCM-s simulations, it is found that the use of the subgrid parameterization always reduces the regional mean precipitation. However, the difference does not appear to have a seasonal dependence. Therefore, the spring and summer drying in the RCM simulation discussed earlier in section 3b(1) is not related to the use of the subgrid parameterization.

Figure 13b shows the model-simulated surface temperature. Except during February, both the RCM-ns and RCM-s simulations are warmer than the CCM3 simu-

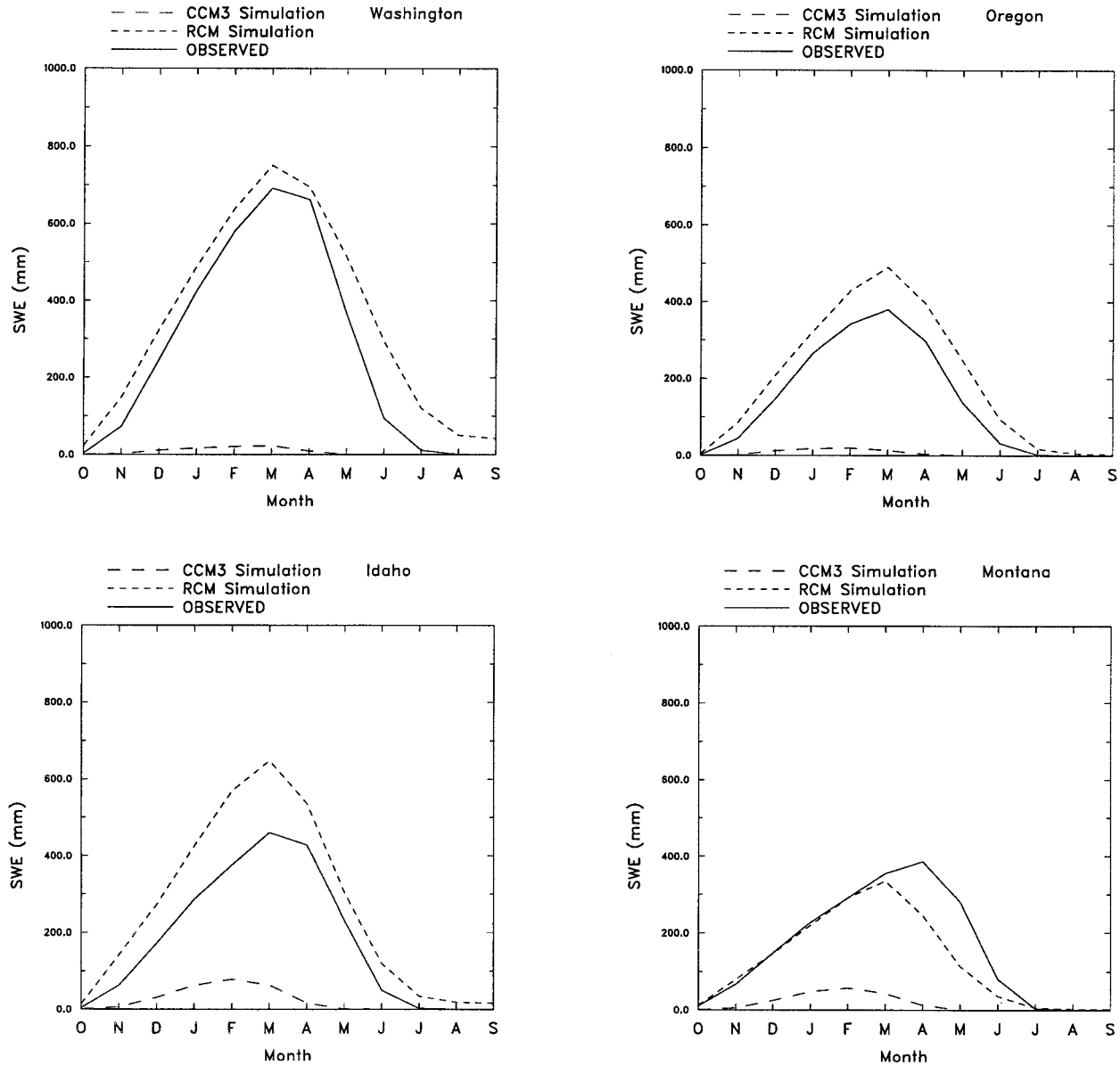

FIG. 12. Similar to Fig. 9 but for SWE averaged over the SNOTEL sites.

lation. This is consistent with the topographic difference in the RCM and CCM3 representations as discussed earlier. It is important to note that both RCM simulations are much warmer than the CCM3 simulation during summer. Again differences between the RCM and CCM3 physical parameterizations, rather than the use of the subgrid parameterization, are more likely to be responsible for this big difference.

Finally, we show the SWE simulated by all the models in Fig. 13c. Clearly, without the use of the subgrid parameterization, the RCM-ns simulation fails to capture the snow cover in the mountainous region of WA during the cold season. Although we expected the RCM-ns simulation to show more snow cover than CCM3 simulation because of its use of higher spatial resolution and the higher precipitation simulated (Fig. 13a), Fig. 13c shows very little difference between the snow simulations. This indicates some clear differences between the surface physics parameterizations used by the two models.

6) STATISTICS

To show the value of using RCM for downscaling, Table 2 lists the statistics of comparing the CCM3 and RCM simulations with observations over the Pacific Northwest. In all cases, the spatial correlation coefficients between the observations and model simulations

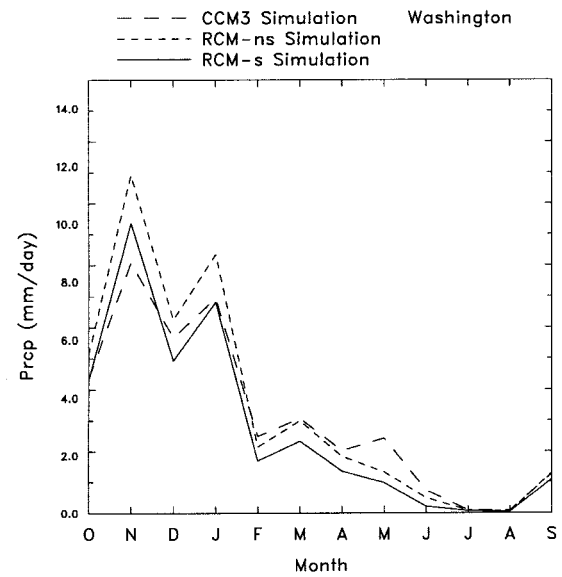

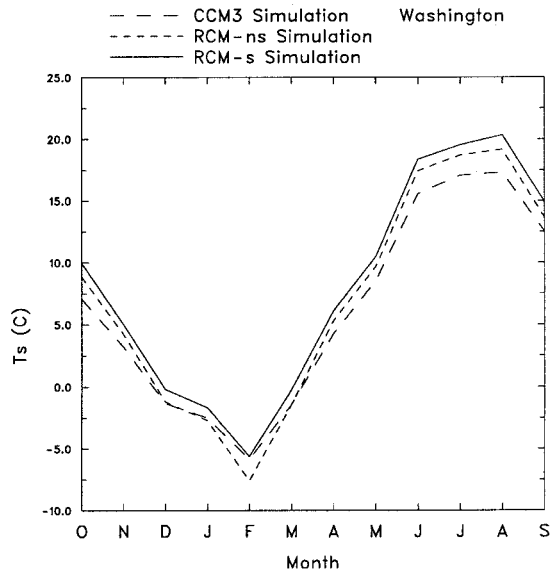

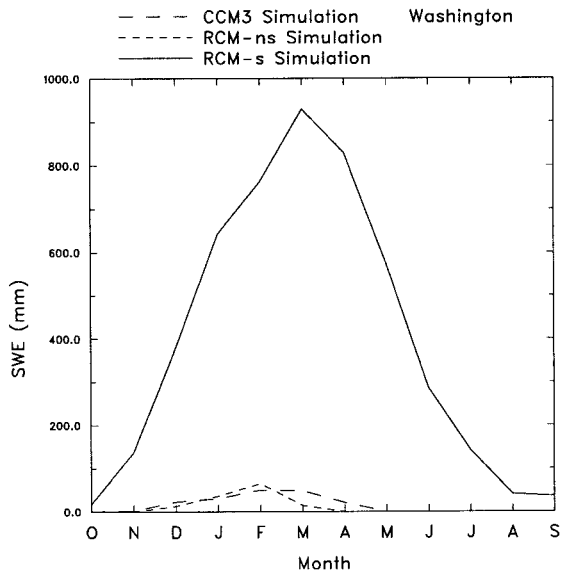

FIG. 13. Regional mean simulations over WA for CCM3 and RCM with (RCM-s) and without (RCM-ns) using the subgrid parameterization of orographic precipitation and land surface cover. Results are shown for (a) precipitation, (b) surface temperature, and (c) snow water equivalent.

TABLE 2. Comparison of mean monthly observed and simulated precipitation (mm day^{-1}) and surface temperature (°C) climatology averaged over four regions for DJF and JJA.

			Precipitation (mm day^{-1})				Surface temperature (°C)			
Season	Statistics	Data	WA	OR	ID	MT	WA	OR	ID	MT
DJF	Mean	OBS	5.07	3.99	1.98	1.04	1.64	1.30	−4.15	−4.74
		CCM3	4.68	4.16	2.70	1.93	−3.39	−1.44	−9.57	−10.33
		RCM	5.26	4.65	3.34	1.41	1.08	0.86	−6.39	−7.15
	Corr	CCM3	0.44	0.51	0.34	0.35	0.63	0.73	0.46	0.03
		RCM	0.70	0.69	0.83	0.72	0.85	0.91	0.83	0.70
JJA	Mean	OBS	1.26	1.06	1.06	1.77	17.61	16.45	16.18	15.98
		CCM3	0.40	0.26	0.83	2.20	17.70	19.80	19.73	16.01
		RCM	0.45	0.27	0.47	1.35	18.20	17.32	17.05	17.62
	Corr	CCM3	−0.36	−0.02	0.54	0.09	−0.11	0.26	0.26	−0.59
		RCM	0.28	0.42	0.67	0.34	0.93	0.91	0.88	0.84

are higher for RCM than CCM3, showing that the RCM simulation reproduces the spatial distribution of surface temperature and precipitation much better than the CCM3. Regional means are harder to judge because the RCM simulation is affected by biases in the CCM3-simulated large-scale circulation. Therefore, regional mean biases in precipitation are sometimes higher for RCM and sometimes lower, depending on the smaller scale features being added on top of the large-scale simulation. For surface temperature, the RCM regional means are always closer to the observed than the CCM3 during winter. During summer, biases are less systematic because a combination of factors (surface topography, vegetation cover, convective and surface physics parameterizations) can alter the simulations to cause differences. Biases in the RCM surface temperature are generally 1°–3°C smaller than those of the CCM3.

It is interesting to note that the CCM3-simulated surface temperature correlates particularly poorly with observations during summer compared with winter. The most likely reason is the crude representation of surface cover defined by CCM3 at the T42 resolution. RCM uses a subgrid elevation/vegetation representation, which explains about 70% of subgrid variations in surface cover defined at 1.5-km resolution. Hence the simulated surface temperature correlates very well with observations even when compared at the locations of the stations. The poor correlation between CCM3 and observed surface temperature during winter over ID and MT may be related to the underprediction of snow in CCM3.

c. Relationships between surface temperature/precipitation and elevation

Both surface temperature and precipitation can vary substantially at different altitudes within a region. Based on this assumption, Leung and Ghan (1995, 1998) developed a subgrid parameterization of orographic precipitation where each RCM grid cell is divided into a number of elevation bands, and surface temperature and precipitation, among many other surface variables, are predicted for each elevation band. To determine how well these variables are simulated over a region, Leung and Ghan compared the model-simulated surface temperature and precipitation with observations at a variety of spatial and temporal scales. Their comparison was based on observations made at about 180 National Weather Service (NWS) surface stations and shorter term simulations within the state of Washington where complex topography is a prominent feature. Here, we evaluate the RCM-simulated surface temperature and precipitation climatology based on the 7-yr simulation driven by the CCM3, and utilize surface temperature and precipitation measurements based on the NWS surface meteorology and SNOTEL stations. Typically, SNOTEL stations are strategically placed at the higher elevation for measurements of snow that are representative of the streamflow. There is a total of 728 surface stations and 270 snotel stations over WA, OR, ID, and MT. About 10% of the NWS stations and 70% of the SNOTEL stations are located above 1500 m, respectively.

Four regions are chosen for this analysis of altitudinal dependence—the Cascades over WA and OR and the northern Rockies range over ID and MT, indicated in Fig. 1. As will be shown, the relationships between precipitation and surface topography are rather distinct within each region. Model simulation is interpolated to the NWS or SNOTEL station locations and elevation according to the method described in section 3b. Relationships between precipitation or surface temperature with altitude are determined by grouping the stations based on their altitude according to the surface elevation classification used in the subgrid precipitation scheme (Table 1). The observed and simulated precipitation are also grouped according to the station altitude, and averaged elevation and precipitation are obtained for each elevation class. Since our focus is on simulating the topographic influence on precipitation, the simulation has been normalized so that the simulated regional mean matches that of the observed. For surface temperature, the regional mean model bias has been subtracted from the simulation. This way, errors in the simulation (as shown in Table 2) that are due to errors in large-scale circulation do not affect the comparison between the observed and simulated precipitation/surface temperature–altitude relationships. Only analysis of the simulation during winter (December–February) will be shown because topography plays an important role in determining wintertime precipitation.

Figure 14a shows the precipitation–altitude relationship over the Cascades range in WA. There is a total of about 120 stations within that area. Surface topography plays a major role in modifying the spatial distribution of precipitation. Typically, during wintertime, precipitation in that area follows synoptic systems that move across the Pacific Ocean, bringing abundant moisture to the Pacific coast. Precipitation is very high at the low lying coastal areas. Between 100 m and 500 m, precipitation decreases with elevation. Most of the stations within this elevation range are located on the leeside of the Cascade, which is affected by rainshadow effect. That is, as precipitation upwind of the mountain depletes moisture in the air, adiabatic descent downwind of the mountain can cause further drying and warming. Rainshadow effect is explicitly represented at the RCM grid scale over the broad range of the Cascades. As surface elevation continues to increase across the Cascades range, precipitation increases as the air flows over mountain barriers, causing a decrease in temperature and increase in condensation. An almost linear relationship is found between precipitation and altitude in this regime between 400 m and 1200 m of altitude.

Above 1500 m, precipitation decreases again for two possible reasons. First, if those stations above 1500 m

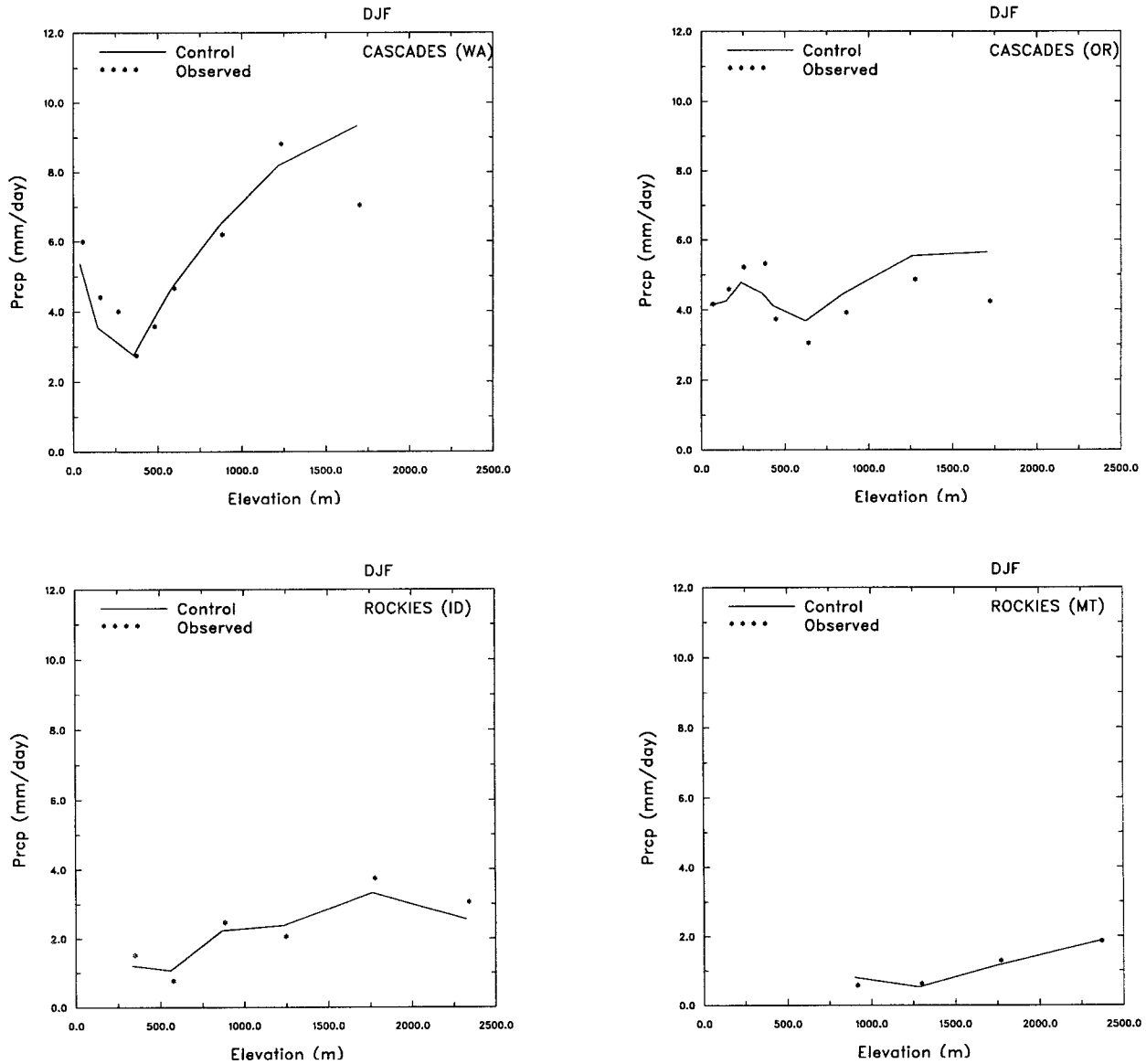

FIG. 14. The observed (asterisks) and simulated (solid line) precipitation as functions of surface elevation within mountain ranges over four different regions: (a) the Cascades over WA, (b) the Cascades over OR, (c) the northern Rockies over ID, and (d) the northern Rockies over MT. Data are aggregated in surface elevation using the subgrid elevation classification shown in Table 1.

are mostly located on the leeward slopes of the mountain, precipitation will likely be lower, even though the stations are located at higher surface elevation. This again is a result of the rainshadow effect. The subgrid orographic precipitation scheme does not account for rainshadow effect within grid cells. Second, if the stations above 1500 m are located further inland than the majority of stations, which are below 1500 m, moisture depletion effect at the lower elevation can again cause drying of the air mass before it encounters higher mountains. Further analysis of the data points above 1500 m indicates that there is a large variability associated with both observations and simulations. At about half of the stations, observed precipitation continues to increase almost linearly beyond 1500 m, and at the other half, precipitation is significantly lower. An example of the former stations was shown in Leung and Ghan (1998) over Mt Rainier. To simulate what happens at the latter stations, a higher grid space resolution would be needed in the RCM. Generally, the model captures the altitude dependence of the observed precipitation very well.

Over the Cascades range in OR, data from about 140 stations are used to generate Fig. 14b. A slightly different precipitation-altitude relationship prevails. This region is typically drier than the Cascades range in WA; the maximum observed precipitation is just about half

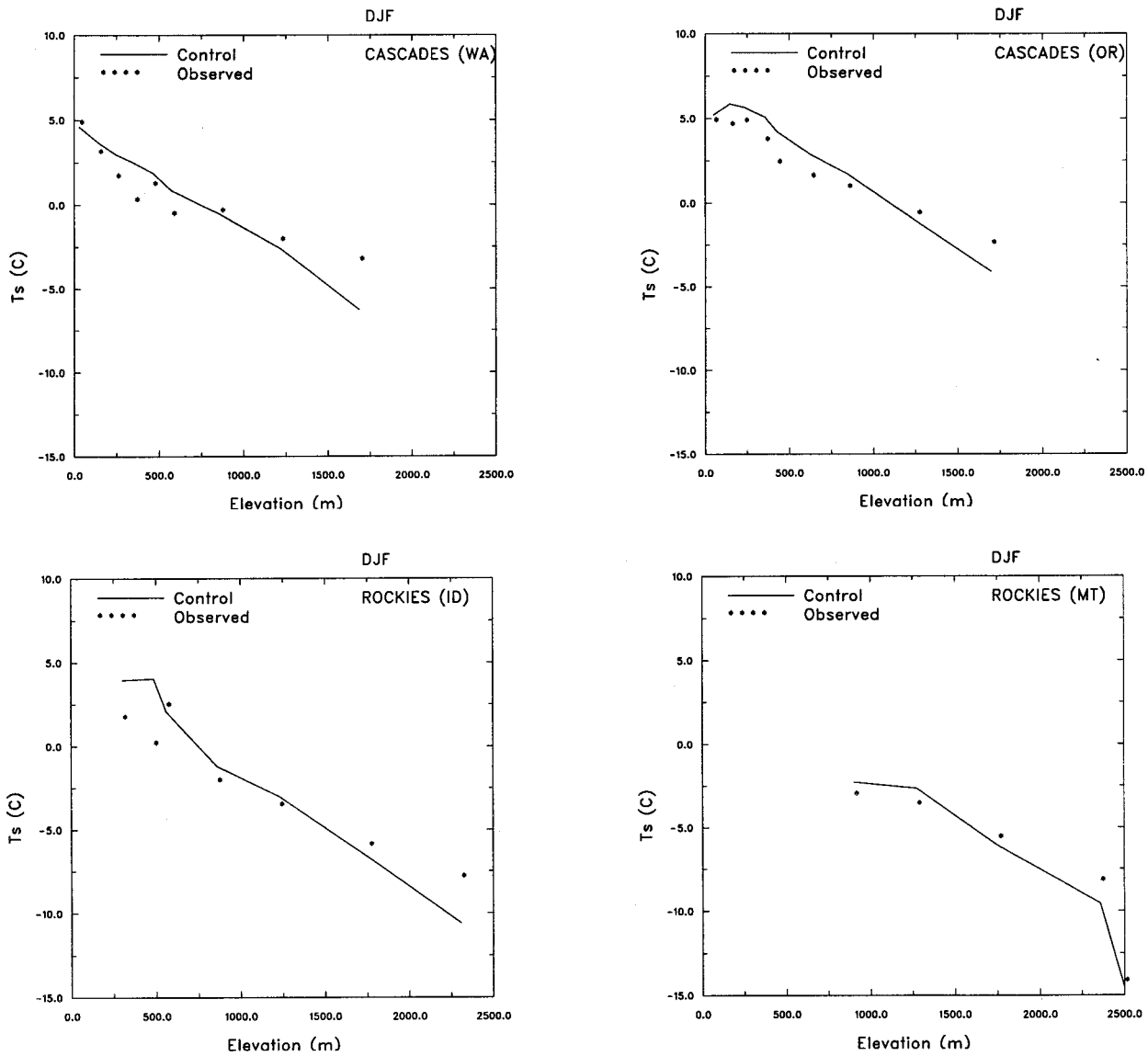

FIG. 15. Similar to Fig. 14 but for surface temperature.

of that in WA. Furthermore, there are two regimes in which precipitation increases with altitude. At the lower elevation, precipitation increases with altitude until about 400 m, after which precipitation decreases to about 600 m. Beyond that, precipitation increases with altitude again, until similar to the Cascades range in WA, precipitation decreases at the higher elevation again above 1500 m. The model simulation is quite close to the observed, except for larger positive biases at the higher elevation.

Over the northern Rockies, observations are available from about 400 m to 2400 m. There are about 65 and 170 stations over ID and MT, respectively. Being much further inland within the continental climate regime, this area is much drier than the Cascades range, with maximum precipitation less than 4 mm day^{-1} during winter. There is a general increase in precipitation as altitude increases. As shown in Figs. 14c and 14d, the model again simulates the precipitation-altitude relationship very well.

Figure 15 shows a similar comparison between the RCM simulation and observation for surface temperature. RCM simulates the changes of surface temperature with elevation rather well over each region. There is, however, a trend for the simulated temperature to be lower than the observed at elevation above 1500 m. This is consistent with the wet bias shown in Fig. 10, especially over the Cascades (WA). Note that the simulation even captures the strong cooling over MT above the 2300-m elevation.

In summary, the range of precipitation variations as functions of topography is highest over the Cascades in

WA. The model is simulating the altitude dependence of precipitation and surface temperature over different regions with different geographic and climate characteristics very well. Similar analyses (not shown) have been performed for the simulation in the summer season. The subgrid parameterizations again reproduced very well the observed altitude dependence of precipitation over the northern Rockies where the relationship varies little from winter to summer. For the Cascades, the observed rate of increase in precipitation with altitude beyond 500 m during summer is only about half that of winter. Our model correctly simulated a lower rate of increase, but only by about 30%. Further improvement is therefore possible; one example is the application of the subgrid parameterizations to finer explicit spatial resolution. The subgrid precipitation and surface temperature information is very useful for coupling regional climate models with hydrology or ecosystem models over mountainous areas where surface hydrology and vegetation processes depend critically on surface topography.

4. Lake simulation

We have selected 14 lakes to be represented in the subgrid surface cover scheme. Here, we evaluate the lake simulation over Pyramid Lake in Nevada and Yellowstone Lake in Wyoming because data are available only for these two lakes. Pyramid Lake is located at 1160 m above sea level and is about 700 km^2 in size and 100 m deep. Yellowstone Lake is about 400 km^2 in size and is 40 m deep and located at 2370 m above sea level.

Figure 16a shows the mean seasonal cycle in lake surface temperature simulated by the model for Pyramid Lake. Observed lake surface temperature is plotted for all data available throughout the simulation period (October 1988–September 1995). From the spread of the data points, we can see that there is quite a range of interannual variability in the lake surface temperature. However, the simulation is clearly too cold when compared with the observation. The bias is between 2° and 3°C in general but higher during spring. This trend is similar to the surface temperature bias as shown in Fig. 12 for most regions. Occasionally over some years, the model simulated a freezing condition between January and April. The averaged ice mass is about 30 kg m^{-2}.

Figure 16b shows a similar comparison of lake surface temperature for Yellowstone Lake. Being located at a higher elevation than the Pyramid Lake, there is a period over 4 months during winter when the lake surface is frozen. The lake surface temperature is simulated quite well, except for a warm bias of 1°–2°C during summer. Maximum ice mass is simulated to be about 400 kg m^{-2}, which occurs in late January. On average, lake ice forms in the beginning of December and lasts until early May in the simulation. The melting of lake ice occurs about 3 weeks earlier than the observations.

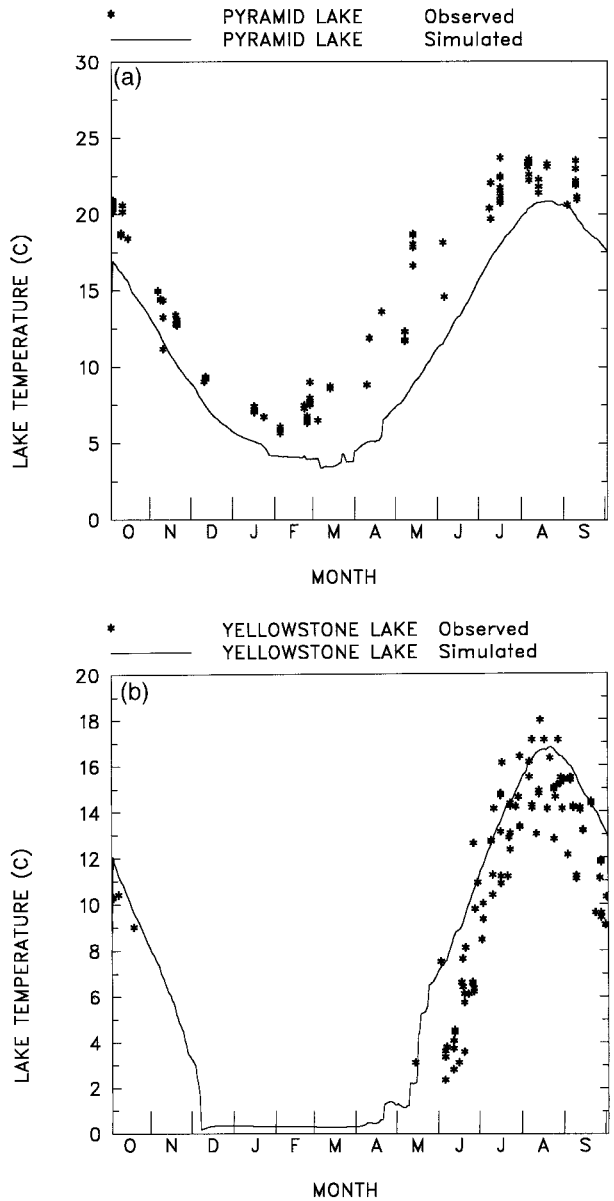

FIG. 16. Simulation of monthly mean lake surface temperature (°C) over (a) Pyramid Lake and (b) Yellowstone Lake and compared with monthly observations.

5. Summary and discussion

Two 7-yr simulations have been performed using a GCM and a RCM, driven by the GCM. Various aspects of the large-scale and regional-scale simulations have been evaluated against observations, and differentiated between the GCM and RCM simulations. Our analyses have focused on the Pacific Northwest where variations in topography and vegetation are important at spatial scales that require the use of regional-scale modeling. Our main conclusions can be summarized as follows:

1) The CCM3 simulation, being performed at T42 resolution, captures quite well the large-scale circulation

when compared with observations. Nevertheless, biases exist that affect the simulated climatology. Most notably, there are biases in the atmospheric temperature that show up as biases in the 500-mb geopotential height. These biases induce northwesterly flow that brings moisture from the Pacific Ocean inland during winter, while during summer, southerly flow is induced along the U.S. west coast that deflects moisture from the Pacific Northwest to California. As a result, there is positive bias up to 2 mm day^{-1} in precipitation over the Pacific Northwest during winter, and in summer, positive bias over California and negative over the Pacific Northwest up to about 1 mm day^{-1}. Surface temperature is mostly too warm except near the southern domain during summer.

2) The RCM-simulated large-scale features are similar to those of CCM3. For example, the difference between the CCM3 and RCM 500-mb geopotential height is within 8 m. Features at the lower atmosphere begin to differ from the CCM3 simulation. These show up in the 850-mb moisture transport, which plays an important role in precipitation over the Pacific Northwest. The RCM simulation shows higher moisture convergence over mountains than CCM3.

3) Precipitation and surface temperature simulated by RCM are affected by errors in the CCM3 large-scale circulation. Hence general biases in the large-scale spatial patterns are similar between the RCM and CCM3 simulation. However, the RCM simulation consistently correlates significantly higher with station observations than the CCM3, showing that the spatial distributions of precipitation and surface temperature are much better simulated by the regional model. Improvements in precipitation simulation are mainly due to the use of more resolved topography; improvements in surface temperature are more likely to be due to more resolved representation in both surface elevation and vegetation used by RCM subgrid topography and vegetation representation. RCM also simulated the SWE in good agreement with observations at the high elevation SNOTEL stations, whereas the CCM3 simulation almost totally missed the SWE. The simulation of surface temperature, precipitation, and SWE at high spatial resolution is important for impact assessment of climate change on water resources and ecosystems.

4) The bias in the regional mean precipitation simulated by RCM is mostly within the observed natural variability of the system. Similar is true for the CCM3 simulation except over MT where the CCM3 simulation is much too high and the bias is above the observed natural variability. This bias is mainly a result of the crude topographic features used in CCM3, which do not exert enough blocking effects on the moisture transport, and hence allow too much moisture to proceed inland.

5) The subgrid parameterization of orographic precipitation and surface cover uses statistical representation of subgrid topograhy and vegetation and, hence, is an efficient modeling alternative to high-resolution modeling to yield good agreement with observation at the more local scale. Our analyses show that variations in precipitation and surface temperature as functions of altitude are well simulated by the subgrid parameterization. However, data are not available at higher elevation to evaluate the relationships at the full range of surface topography present at the Pacific Northwest.

Although areas above 2000 m are relatively small, they still contribute about 17% of the area over the Pacific Northwest study region (Table 1). Precipitation at high elevation is important, because snow accumulation over the high elevation is an important source of water for spring and summer streamflow. Distributed hydrology models, after being calibrated with observed meteorology, could be a useful tool for evaluating the spatial distribution of model-simulated precipitation. Although correct simulation of the watershed mean precipitation may be enough to simulate the annual streamflow, biases in the simulation of precipitation–altitude relationships will readily appear as biases in the timing of the streamflow, because the former govern how much precipitation is stored as snow for spring or summer release.

Leung et al. (1996) used a regional climate simulation to drive a distributed hydrology model over the Middle Fork Flathead watershed in Montana and found good agreement between observed and simulated streamflow. The Middle Fork Flathead watershed is located at very high elevation so that precipitation during winter is mostly in the form of snow. Watersheds located at the more modest elevation that crosses snowline would require higher accuracy in the simulation of precipitation–altitude relationships for correct simulation of the timing and amount of streamflow. Therefore, it remains to be tested whether the kind of accuracy as seen in the simulation of relationships between precipitation–surface temperature with altitude is enough for hydrological or ecological modeling at the watershed scales in mountainous areas.

Acknowledgments. This work was supported by the U.S. Environmental Protection Agency, National Center for Environmental Research and Quality Assurance, Grant R82-4803-010 to the Pacific Northwest National Laboratory (PNNL). We want to thank the National Center for Atmospheric Research for making the CCM3 available for our simulation. We also thank the Program for Climate Model Diagnostics and Intercomparison at the Lawrence Livermore National Laboratory for sharing the AMIP SST and sea ice data. PNNL is operated for the U.S. Department of Energy by Battelle Memorial Institute under Contract DE-AC06-76RLO 1830.

REFERENCES

Anthes, R. A., E. Y. Hsie, and Y. H. Kuo, 1987: Description of the Penn State/NCAR Mesoscale Model version 4 (MM4). NCAR Tech. Note NCAR/TN-282+STR, 66 pp.

Bonan, G. B., 1996: A land surface model (LSM version 1.0) for ecological, hydrological and atmospheric studies: Technical description and user's guide. NCAR Tech. Note NCAR/TN-417+STR, 150 pp.

Briegleb, B. P., 1992: Delta–Eddington approximation for solar radiation in the NCAR Community Climate Model. *J. Geophys. Res.,* **97,** 7603–7612.

Cotton, W. R., G. J. Tripoli, R. M. Rauber, and E. A. Mulvihill, 1986: Numerical simulation of the effects of varying ice crystal nucleation rates and aggregation processes on orographic snowfall. *J. Climate Appl. Meteor.,* **25,** 1658–1680.

Dickinson, R. E., A. Henderson-Sellers and P. J. Kennedy, 1993: Biosphere–atmosphere transfer scheme (BATS) version 1e as coupled to the NCAR Community Climate Model. NCAR Tech. Note NCAR/TN-387+STR, 72 pp.

Ghan, S. J., and R. C. Easter, 1992: Computationally efficient approximations to stratiform cloud parameterization. *Mon. Wea. Rev.,* **120,** 1572–1582.

Giorgi, F., and G. T. Bates, 1989: The climatological skill of a regional model over complex terrain. *Mon. Wea. Rev.,* **117,** 2325–2347.

——, M. R. Marinucci, G. T. Bates, and G. DeCanio, 1993: Development of a second-generation regional climate model (RegCM2). Part II: Convective processes and assimilation of lateral boundary conditions. *Mon. Wea. Rev.,* **121,** 2814–2832.

——, C. S. Brodeur, and G. T. Bates, 1994: Regional climate change scenarios over the United States produced with a nested regional climate model. *J. Climate,* **7,** 375–399.

Grell, G., 1993: Prognostic evaluation of assumptions used by cumulus parameterizations. *Mon. Wea. Rev.,* **121,** 764–787.

——, J. Dudhia, and D. R. Stauffer, 1993: A description of the fifth-generation Penn State/NCAR Mesoscale Model (MM5). NCAR Tech. Note NCAR/TN-398+IA, 107 pp.

Hack, J. J., 1994: Parameterization of moist convection in the National Center for Atmospheric Research Community Climate Model (CCM2). *J. Geophys. Res.,* **99,** 5551–5568.

——, J. T. Kiehl, and J. W. Hurrell, 1998: The hydrologic and thermodynamic characteristics of the NCAR CCM3. *J. Climate,* **11,** 1179–1206.

Hirakuchi, H., and F. Giorgi, 1995: Multi-year present day and $2\times CO_2$ simulations of monsoon climate over eastern Asia and Japan with a regional climate model nested in a general circulation model. *J. Geophys. Res.,* **100,** 21 105–21 126.

Holtslag, A. A. M., and B. A. Boville, 1993: Local versus nonlocal boundary-layer diffusion in a global climate model. *J. Climate,* **6,** 1825–1842.

Hostetler, S., and P. J. Bartlein, 1990: Simulation of lake evaporation with application to modeling lake level variations in Harney-Malheur Lake, Oregon. *Water Resour. Res.,* **26,** 2603–2612.

Hurrell, J. W., J. J. Hack, B. A. Boville, D. L. Williamson, and J. T. Kiehl, 1998: The dynamical simulation of the NCAR Community Climate Model version 3 (CCM3). *J. Climate,* **11,** 1207–1236.

IPCC, 1996: *The Science of Climate Change. Climate Change 1995,* J. T. Houghton et al. Eds. Cambridge University Press, 572 pp.

Kiehl, J. T., R. J. Wolski, B. P. Briegleb, and V. Ramanathan, 1987: Documentation of radiation and cloud routines in the NCAR Community Climate Model (CCM1). NCAR Tech. Note NCAR/TN-288+IA, 105 pp.

——, J. J. Hack, G. B. Bonan, B. A. Boville, B. P. Briegleb, D. L. Williamson, and P. J. Rasch, 1996: Description of the NCAR Community Climate Model (CCM3). NCAR Tech. Note NCAR/TN-420+STR, 152 pp.

——, ——, ——, ——, D. L. Williamson, and J. W. Hurrell, 1998a: The National Center for Atmospheric Research Community Climate Model: CCM3. *J. Climate,* **11,** 1131–1149.

——, ——, and J. W. Hurrell, 1998b: The energy budget of the NCAR Community Climate Model: CCM3. *J. Climate,* **11,** 1151–1178.

Legates, D. R., and C. J. Willmott, 1990a: Mean seasonal and spatial variability in gauge-corrected global precipitation. *Int. J. Climatol.,* **10,** 111–127.

——, and ——, 1990b: Mean seasonal and spatial variability in global surface air temperature. *Theor. Appl. Climatol.,* **41,** 11–21.

Leung, L. R., and S. J. Ghan, 1995: A subgrid parameterization of orographic precipitation. *Theor. Appl. Climatol.,* **52,** 95–118.

——, and ——, 1998: Parameterizing subgrid orographic precipitation and land surface cover in climate models. *Mon. Wea. Rev.,* **126,** 3271–3291.

——, M. S. Wigmosta, S. J. Ghan, D. J. Epstein, and L. W. Vail, 1996: Application of a subgrid orographic precipitation/surface hydrology scheme to a mountain watershed. *J. Geophys. Res.,* **101,** 12 803–12 817.

Marshall, S., J. O. Roads, and R. J. Oglesby, 1997: Effects of resolution and physics on precipitation in the NCAR Community Climate Model. *J. Geophys. Res.,* **102,** 19 529–19 541.

McFarlane, N. A., 1987: The effect of orographically excited wave drag on the general circulation of the lower stratosphere and troposphere. *J. Atmos. Sci.,* **44,** 1775–1800.

McGregor, J. L., and K. J. Walsh, 1993: Nested simulations of perpetual January climate over the Australian region. *J. Geophys. Res.,* **98,** 23 283–23 290.

——, and ——, 1994: Climate change simulations of Tasmanian precipitation using multiple nestings. *J. Geophys. Res.,* **99** (D10), 20 889–20 905.

Patterson, J. C., and P. F. Hamblin, 1988: Thermal equilibrium of a lake with winter ice cover. *Limnol. Oceanogr.,* **33,** 323–338.

Risbey, J. S., and P. H. Stone, 1996: A case study of the adequacy of GCM simulations for input to regional climate change assessments. *J. Climate,* **9,** 1441–1467.

Shea, D. J., K. E. Trenberth, and R. W. Reynolds, 1990: A global monthly sea surface temperature climatology. NCAR Tech. Note NCAR/TN-345+STR 167 pp.

Taylor, K. E., and S. J. Ghan, 1992: An analysis of cloud liquid water feedback and global climate sensitivity in a general circulation model. *J. Climate,* **5,** 907–919.

——, D. Williamson, and F. Zwiers, 1997: AMIP II sea surface temperature and sea ice concentration boundary conditions. [Available online at http://www-pcmdi.llnl.gov/amip/AMIP2EXPDSN/BCS/amip2bcs.html.]

Williamson, D. L., and P. J. Rasch, 1994: Water vapor transport in the NCAR CCM2. *Tellus,* **46A,** 34–51.

Zhang, D. L., and R. A. Anthes, 1982: A high-resolution model of the planetary boundary layer–sensitivity tests and comparisons with SESAME-79 data. *J. Appl. Meteor.,* **21,** 1594–1609.

Zhang, G. J., and N. A. McFarlane, 1995: Sensitivity of climate simulations to the parameterization of cumulus convection in the Canadian Climate Centre General Circulation Model. *Atmos.–Ocean,* **33,** 407–446.